Author/s:
Zhang, J;Jiang, WJ;Niu, S;Zhang, H;Liu, J;Li, H;Huang, GF;Jiang, L;Huang, WQ;Hu, JS;Hu, W

Title:
Organic Small Molecule Activates Transition Metal Foam for Efficient Oxygen Evolution Reaction

Date:
2020-03-01

Citation:
Zhang, J., Jiang, W. J., Niu, S., Zhang, H., Liu, J., Li, H., Huang, G. F., Jiang, L., Huang, W. Q., Hu, J. S. & Hu, W. (2020). Organic Small Molecule Activates Transition Metal Foam for Efficient Oxygen Evolution Reaction. Advanced Materials, 32 (11), https://doi.org/10.1002/adma.201906015.

Persistent Link:
https://hdl.handle.net/11343/275379

DOI: 10.1002/((please add manuscript number))

Article type: Communication

Organic Small Molecule Activates Transition Metal Foam for Efficient Oxygen Evolution Reaction

Jing Zhang, Wen-Jie Jiang, Shuai Niu, Hantang Zhang, Jie Liu, Haiyang Li, Gui-Fang Huang, Lang Jiang, Wei-Qing Huang*, Jin-Song Hu*, and Wenping Hu*

J. Zhang, Prof. W.-Q. Huang, Prof. G.-F. Huang

Department of Applied Physics, School of Physics and Electronics, Hunan University, Changsha 410082, China

E-mail: wqhuang@hnu.edu.cn

J. Zhang, H. Li, Prof. J. Liu, Prof. L. Jiang

Beijing National Laboratory for Molecular Sciences (BNLMS), Key Laboratory of Organic

Solids, Institute of Chemistry, Chinese Academy of Sciences (CAS), Beijing 100190, China

E-mail: ljiang@iccas.ac.cn

S. Niu, Dr. W.-J. Jiang, Prof. J.-S. Hu

Beijing National Laboratory for Molecular Sciences (BNLMS), CAS Key Laboratory of Molecular Nanostructure and Nanotechnology, Institute of Chemistry, Chinese Academy of Sciences, Beijing 100190, China

E-mail: hujs@iccas.ac.cn

J. Zhang, S. Niu, H. Li, Prof. J. Liu, Prof. L. Jiang, Prof. J.-S. Hu

University of Chinese Academy of Sciences, Beijing 100049, China

Dr. H. Zhang

College of Chemistry and Material Science, Shandong Agricultural University, Taian 271018, Shandong, China

Prof. W. Hu

Tianjin Key Laboratory of Molecular Optoelectronic Sciences, Department of Chemistry, School of Science, Tianjin University and Collaborative Innovation Center of Chemical Science and Engineering, Tianjin 300072, China

Keywords: transition metal nanomesh, graphene-like film, solid-phase migration, hexabromobenzene, oxygen evolution reaction

Abstract

Developing low-cost, highly-efficient and durable electrocatalysts for oxygen evolution reaction (OER) is essential for the practical application of electrochemical water splitting. Herein, we discover that organic small molecule (hexabromobenzene, HBB) can activate commercial transition metal foam (Ni, Fe, and NiFe foam) for efficient OER by directly evolving transition metal nanomeshes embedded in graphene-like films (M-NM@G) through a facile Br-induced solid-phase migration process. Systematic investigations indicate that HBB can conformally generate graphene-like network on bulk transition metal foam substrate via the cleavage of C-Br bonds and the formation of C=C linkage. Simultaneously, the cleaved C-Br fragments can efficiently extract metal atoms from bulk substrate, in-situ producing transition metal nanomeshes embedded in the graphene-like films. Graphene-like film can not only protect metal foam from corrosion but also hold the better oxidation-resistance during OER compared with other carbon substrates. Nanomeshed transition metal can evolve sufficient active sites during OER while its integration in graphene-like film makes it mechanically stable. As a result, such functional nanostructure can serve as an efficient OER electrocatalyst with a low overpotential and excellent long-term stability. Specifically, the overpotential at 100 mA cm^{-2} is only 208 mV for NiFe-NM@G, ranking the top-tier OER electrocatalysts. This work demonstrates an intriguing general strategy for directly transforming bulk transition metals into nanostructured functional electrocatalysts via the interaction with organic small molecules, opening up opportunities for bridging the application of organic small molecules in energy technologies.

Environment-friendly and low-cost energy conversion and storage devices have received increasing attention due to the vast demand for clean energy.[1] Hydrogen as an ideal clean energy carrier is playing more and more important role in clean energy conversion and utilization. One of the big challenges for hydrogen economics is the low-cost mass production of high-purity hydrogen. Electrochemical water splitting is a practical and scalable technique to produce hydrogen with high purity and can be integrated with other renewable energy sources such as solar/wind energy.[2] However, compared with the cathode reaction (hydrogen evolution reaction, HER), the anode reaction (oxygen evolution reaction, OER) is much more sluggish due to multiple proton-coupled electron transfer processes and typically requires a high overpotential to overcome.[3] To date, precious-metal-based catalysts such as Ir/Ru are well known to exhibit remarkable catalytic activity for OER, but their high cost and rarity pose a significant limitation in its large-scale industrial applications.[4] Therefore, it is highly demanded to exploit cost-effective, earth-abundant, and efficient OER electrocatalysts with comparable catalytic activity to noble metal for water splitting.

In the last few decades, transition metal-based catalysts, especially nickel-based materials, including nickel oxides,[5] nickel-hydroxide,[6] nickel-oxyhydroxide,[7] nickel sulfides[3a, 8] and Ni-based layer double hydroxide,[9] have been reported as promising catalytically active sites due to their low cost, easy availability, and high catalytic activity. For example, a small overpotential of 331 mV was achieved to output current density of 10 mA cm^{-2} on nanostructured α-nickel-hydroxide for OER.[6b] Besides, Xu *et al.* successfully developed metallic Ni_3N nanosheets as an efficient OER electrocatalyst, which exhibited superior catalytic activity compared with bulk Ni_3N and NiO nanosheets.[10] Nevertheless, there are still two main challenges standing in the way of practical application of nickel-based materials in water splitting: less-satisfied catalytic activity and durability

especially under high current density.[6a, 10-11] Most of reported nickel-based materials (oxides, hydroxides) have low conductivity and have to be coupled with other conductive materials such as carbon. In addition, the OER electrocatalysts in form of powders will easily peel off under high current density when they are coated on conductive substrate with polymeric binders. It is still challenging to develop a simple strategy to figure out these two issues simultaneously, thus facilitating the application of nickel-based OER electrocatalysts in water splitting.

Herein, we discover that Br-containing organic small molecule such as hexabromobenzene (HBB) enables a "top-down"[12] solid-phase migration method to directly produce transition metal nanomeshes well-embedded in graphene-like film (M-NM@G) on commercial transition metal foam substrate. Systematic experiments indicate that such intriguing solid-phase migration phenomenon is related with bromine in HBB. This special structure possesses several advantages for OER: 1) The solid-phase migration of transition metal atoms directly from substrate to form nanomeshes guarantees the tight connection between them and thus stable operation at high current density; 2) The nanomesh structure has porous structure and relatively large surface area for exposing sufficient accessible active sites; 3) Graphene-like film directly grown on substrate protects transition metal foam from corrosion and has better oxidation-resistance during OER compared with other carbon substrates during OER; 4) The embedding of transition metal nanomeshes in the graphene-like film ensures the excellent conductivity and mechanically stability for Ni-evolved OER active sites during operation. As a result, the as-prepared M-NM@G exhibits superior OER performance with a low overpotential for three catalysts as well as outstanding long-term stability. Especially for NiFe-NM@G, the overpotential at 100 mA cm^{-2} is only 208 mV, which is the best reported performance. This strategy provides a promising way to directly transform bulk transition metals into

nanostructures and enable commercial transition metal foam to directly serve as highly efficient electrode for OER.

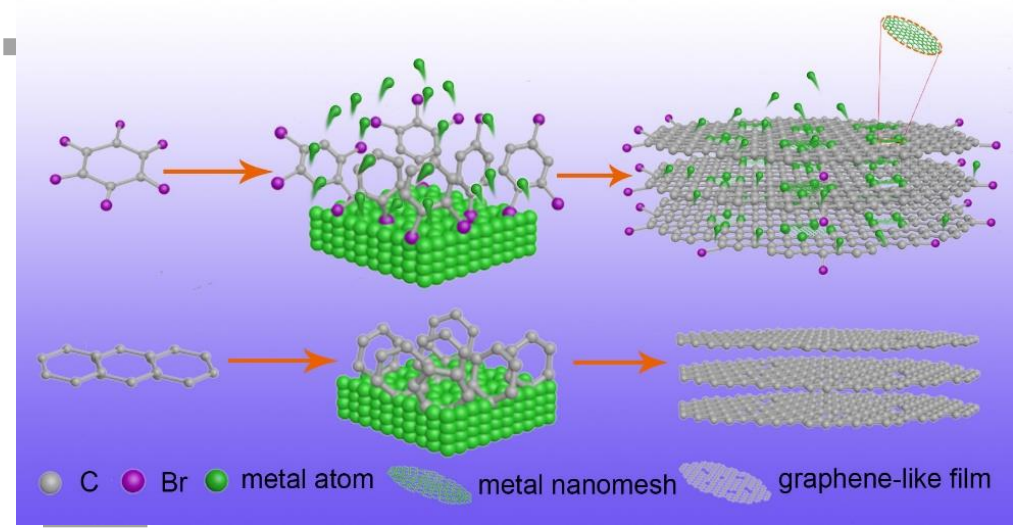

Scheme 1. Scheme of solid-phase migration process for forming M-NM@G catalyst.

The fabrication process of M-NM@G is depicted in **Scheme 1** and the details are described in the Experimental Section. In brief, a piece of HBB flake is put on upstream and the transition metal foam is put on the downstream. Based on our previous work,[13] the C-Br bonds of HBB could be dissociated into some carbon derivatives under low temperature. Thus, the C-Br bonds effectively rupture due to the sublimation of HBB under 550 ^{o}C, and then are transported with the carrier gas of Ar, resulting in C=C linkage to generate graphene-like network on transition metal substrate. Meanwhile, transition metal atoms are extracted out from the bulk transition metals under bromine atmosphere, in-situ forming transition metal nanomeshes uniformly embedded in the graphene-like films. In contrast, no transition metal nanomeshes could be formed when using another carbon

source (anthracene) without C-Br bonds to replace HBB in the upstream. Therefore, bromine plays a key role to directly transform bulk transition metals into nanomeshes during this process.

The morphology and elemental analysis of Ni-NM@G were first examined by scanning electron microscopy (SEM). The morphology of Ni-NM@G varies with the growth temperature and time. The SEM images of the products prepared under 550 ^{o}C for 1 h and 5 h (denoted as Ni-NM@G-1, and -5, respectively) are shown in Figure S1. It can be seen that uniform film

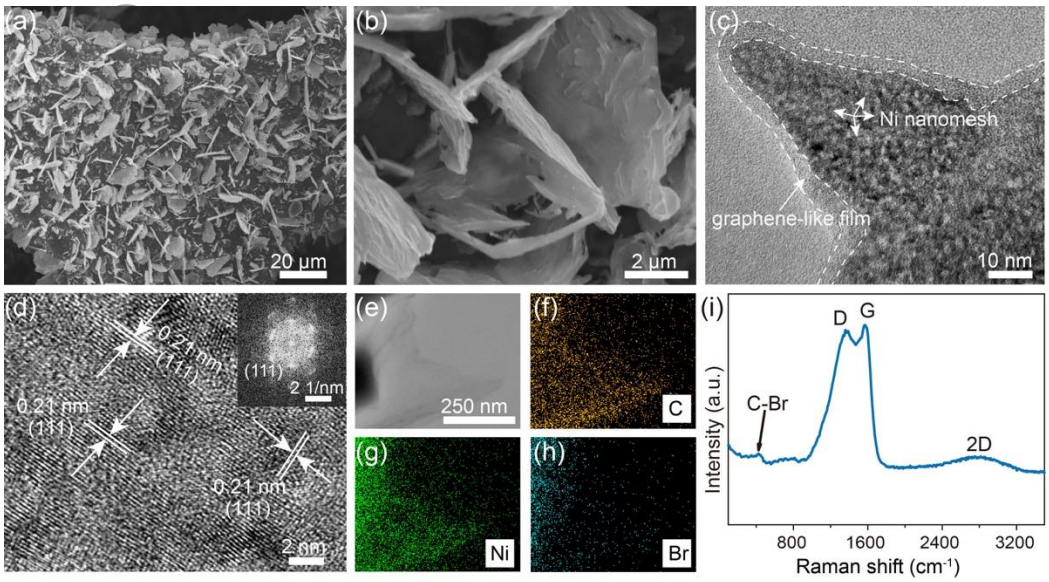

Figure 1. (a, b) SEM images, (c) TEM image, (d) HRTEM image, (e-h) STEM image and corresponding elemental mapping, and (i) Raman spectrum of Ni-NM@G-10 catalyst.

covers on the whole surface of nickel foam for Ni-NM@G-1 (Figure S1a). When the growth time increases to 5 h, some flakes appear and vertically stand on the top of film for Ni-NM@G-5 (Figure S1b). With the increase of growth time to 10 h (denoted as Ni-NM@G-10), more flakes vertically grow on the surface of the film covering on the top of film as shown in **Figure 1**a. High-resolution SEM image (**Figure 1**b) shows the rough surfaces of these flakes with included metal in high contrast.

Transmission electron microscopy (TEM) was further performed to gain insights into the microstructures of Ni-NM@G at different growth time. As shown in Figure S2, nickel nanoparticles are produced at the initial growth stage and gradually interconnected to form nickel nanomeshes with the increase of growth time. When the growth time reaches 10 h (Ni-NM@G-10), there are numerous interconnected nanoparticles, forming nanomeshes morphology (**Figure 1**c). Besides, a thin layer with light contrast (as indicated by dash lines) embedding the nanomeshes can be clearly observed. According to our previous work, the C-Br bonds in HBB molecules could effectively rupture under high temperature and result in C=C linkage to form graphene-like network.[13] Therefore, the thin layer could be suspected to be graphene-like carbon. The structure of Ni-NM@G-10 is further examined by high-resolution TEM (HRTEM). Clearly, the distinct lattice spacing of 0.21 nm is easily observed in various areas (**Figure 1**d), which can be well assigned to (111) crystal planes of metallic Ni.[1e] The corresponding fast Fourier transform (FFT) pattern corroborates the existence of metallic Ni (inset in **Figure 1**d). The elemental mapping images in **Figure 1**e-h clearly show the uniform distribution of Ni, C and Br element in a graphene-like flake embedding Ni nanomeshes. Furthermore, the Raman spectrum of Ni-NM@G-10 catalyst was shown in **Figure 1**i. The well-known D, G and 2D bands at 1360.4, 1587.5 and 2772.6 cm^{-1} are clearly observed.[14] The D band corresponds to the structural defects of lattice symmetry. The G band is associated with the characteristic of the sp^2 hybridization of carbon. While the relatively weak and broad 2D band indicates there are some defects in Ni-NM@G. Besides, a small peak at 425.5 cm^{-1} is assigned to C-Br bond, indicating Br doping is achieved during the C=C linkage process. The Fourier Transform Infrared (FTIR) spectroscopy was carried out to detect functional groups in the catalyst. As shown in Figure S3, the peak around 567 cm^{-1} can be attributed to the C-Br stretching vibration, corroborating

the presence of C-Br species in the catalyst. The peaks at 866, 1164, 1419, 1622, and 3259 cm^{-1} were contributed to Ni-O vibrations, C-O-C, OH-bending, C=C bond, and OH-stretching, respectively.[15] Based on above evidences, it can be concluded that the produced Ni-NM@G-10 films are composed of nickel nanomeshes embedded in Br-doped graphene-like layer.

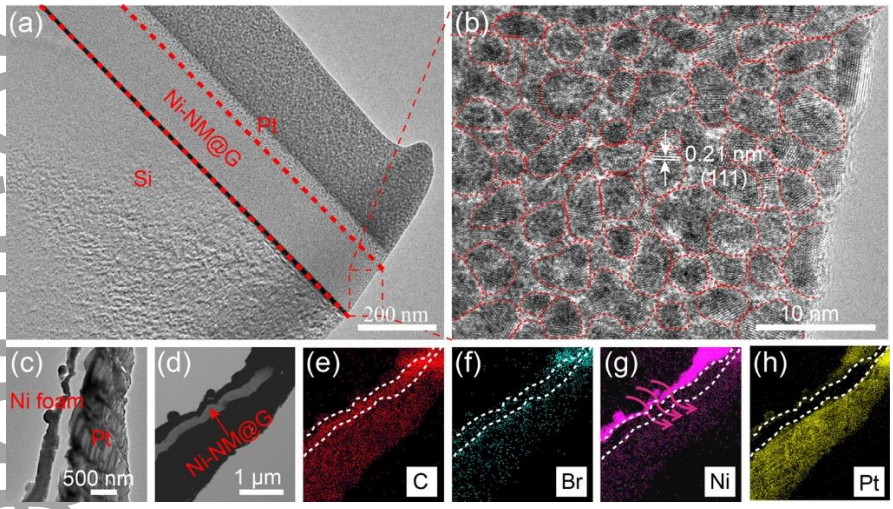

Figure 2. Cross-sectional (a) TEM and (b) HRTEM images of a single layer of Ni-NM@G-10 nanomeshes. (c-h) TEM image and corresponding elemental mapping images of the Ni-NM@G-10 film covering on the surface of nickel foam.

To confirm the distribution of nickel nanomeshes in the vertical direction, the cross-sectional TEM of Ni-NM@G-10 was performed using focused ion beam (FIB) technique. As shown in **Figure 2**a, a single layer of Ni-NM@G-10 was shown with a thickness of approximately 135 nm. Furthermore, the HRTEM image shows that a plenty of interconnected nickel nanoparticles (3-4 nm in diameter) are uniformly embedded in graphene-like film (**Figure 2**b), forming nickel nanomeshes. The distinct lattice fringe distance was indexed to the (111) planes of Ni. Meanwhile, the cross-sectional bright-field TEM image of Ni-NM@G-10 film covering on the surface of Ni foam exhibits a less conductive layer grown on Ni foam (**Figure 2**c and d). As shown in **Figure 2**e-h, elemental mapping analyses validates the signals from C, Ni, Br elements which are uniformly distributed in the layer,

corroborating the homogeneous distribution of Ni nanomeshes in the Ni-NM@G-10 film. The Pt signal on outside the layer is from the deposited Pt for the sample preparation via FIB technique. Close observation on Ni mapping image shows that the Ni signal is getting slightly weak from Ni foam substrate to outside (**Figure 2**g), implying that Ni migrates from Ni foam and gets into carbon layer to form Ni nanomeshes.

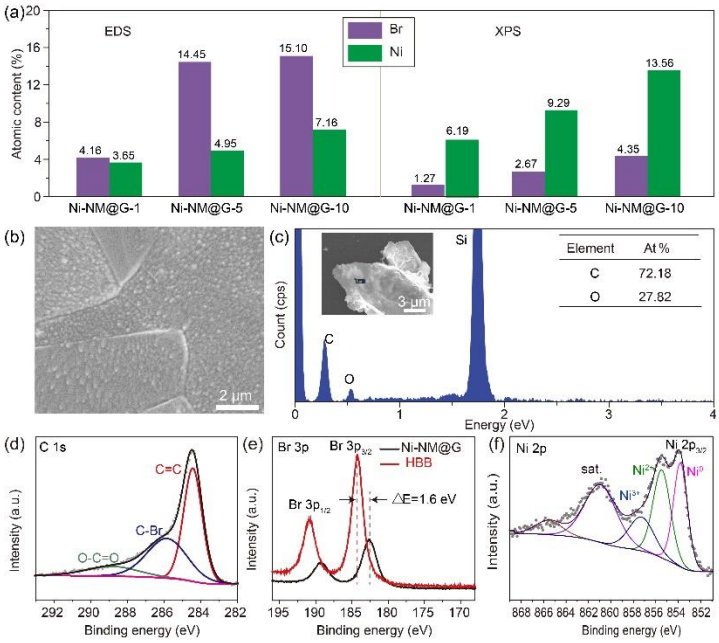

Figure 3. (a) The atomic contents of Br and Ni in Ni-NM@G prepared at different growth stages, calculated from both EDS and XPS results. (b-c) SEM image and EDS spectrum of An@G. (d) C 1s, (e) Br 3p, and (f) Ni 2p XPS spectra of Ni-NM@G-10.

To explore the formation mechanism of nickel nanomeshes through the solid-phase migration, the compositions of products at different growth time were examined. Energy-dispersive X-ray spectroscopic (EDS) spectra of as-produced catalysts were recorded on the sample prepared by ultrasonically exfoliating nickel nanomeshes and drop-casting them on Si/SiO_2 wafer to rule out the effect of Ni foam substrate. Only C, Br and Ni elements are detected in all samples (Figure S4). Notably, the signal of Br and Ni become much stronger with the increase of growth time. The

contents of Ni and Br elements in the samples at different growth times are shown in **Figure 3**a. The Ni content increases with the increase of Br content. The similar tendency can also be seen in the results based on the elemental analyses from X-ray photoelectron spectroscopy (XPS). Both SEM and TEM have shown that nickel nanomeshes are formed with the increase of growth time. Combing these results, it can be concluded that the solid-phase migration of Ni atoms from Ni foam substrate should be related with the active Br species cleaved from HBB. To further support this point, anthracene (An) without Br was applied as carbon source to replace HBB while keeping all other experimental conditions same. The obtained control sample was denoted as An@G. As shown in **Figure 3**b, only a layer of film is obtained to cover the whole surface of Ni foam. No flakes are found to grow on the film. The elemental analyses based on SEM-EDS find only C and O elements without detectable Ni signal (**Figure 3**c). Besides, XPS spectra (Figure S5) shows that only C, O and Ni elements are present on the surface of An@G, consistent with EDS results. The Ni signal is from the Ni foam substrate. This result confirms that the solid-phase migration of Ni is indeed accomplished by active Br species under suitable temperature. Another control experiment was carried out by further elevating the processing temperature to 600 ^{o}C. According to our previous study,[13] too high growth temperature will cause the evaporation of Br and the less residue in the graphene-like film. As shown in Figure S6 and S7, no obvious flakes with Ni nanomeshes is observed. As expected, Br content in the film grown at 600 ^{o}C is much less that at 550 ^{o}C, leading to the much less Ni content (Figure S8). This result further confirms the correlation between the solid-phase migration of Ni atoms and active Br species from the cleavage of HBB molecules.

The surface elemental composition and electronic states of Ni-NM@G-10 was probed by XPS. As shown in Figure S9, the characteristic peaks of C, Br and Ni indicate these elements exist in Ni-

NM@G-10, consistent with the EDS results. The high-resolution XPS spectrum of C 1s (**Figure 3**d) shows that there is one broad peak at the binding energy of 284.4 eV, which can be well fitted with three peaks at 284.4, 286.3, and 289.3 eV, corresponding to C=C (sp^2), C-Br, and O-C=O, respectively.[14] The small peak of O-C=O species is mainly due to the physical adsorption of oxygen-containing molecule from air. Moreover, as shown in **Figure 3**e, two obvious peaks at 184.2 and 190.8 eV in high-resolution Br $3p_{3/2}$ and Br $3p_{1/2}$ XPS spectrum are the typical peaks of C-Br bonds.[16] It should be noted that an obvious shift (~1.6 eV) is observed for powder HBB and Ni-NM@G, indicating the change in the electronic structure of Ni-NM@G. This result indicates that there should a strong interaction between Ni and Br. The Ni $2p_{3/2}$ spectrum shows three peaks located at the binding energies of 853.6, 855.4 and 857.2 eV (**Figure 3**f), corresponding to metallic Ni, Ni^{2+} and Ni^{3+}, respectively.[5] The result confirms the existence of Ni element while the oxidative state should be come from the surface oxidation of metallic Ni.

The electrocatalytic activities of Ni-NM@G toward OER was tested using a three-electrode system in 1.0 M KOH electrolyte at a scan rate of 2 mV s^{-1}. In **Figure 4**a, the bare Ni foam and An@G exhibit negligible OER activity compared with superior activity of the Ni-NM@G. With the increase of the growth time, the OER performance of Ni-NM@G catalysts gradually increase and reach the highest activity at the growth time of 10 h. The Ni-NM@G-10 catalyst shows the lowest overpotential of 318 mV at a high current density of 100 mA cm^{-2}, which is much lower than those of unary or even some binary nickel-based catalysts, including nickel foam (485 mV),[17] MIL-53(Ni)/NF (520 mV),[17] NiCo@$NiCoO_2$/C PMRAs (440 mV),[18] MWCNTs/$Ni(OH)_2$ (870 mV),[6a] NiCo-LDH nanosheets (>400 mV),[19] $NiCo_2O_4$

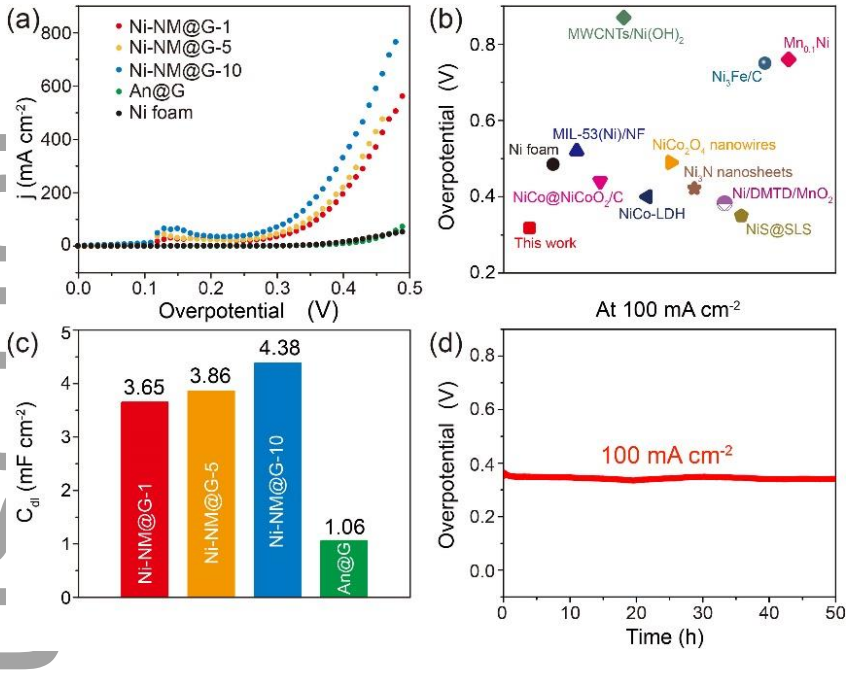

Figure 4. (a) OER polarization curves in deaerated 1.0 M KOH solution at a scan rate of 2.0 mV s^{-1}. (b) The overpotential of Ni-NM@G in comparison with reported Ni-based catalysts. (c) C_{dl} values of as-prepared catalysts. (d) Time-dependent current density curve for Ni-NM@G-10 in 1.0 M KOH.

nanowires (490 mV),[20] Ni/DMTD/MnO_2 (422 mV),[21] Ni_3N nanosheets (390 mV),[10] NiS@SLS (350 mV),[22] Ni_3Fe/C (>750 mV),[1e] and $Mn_{0.1}Ni$ (>760 mV), etc.[23] The comparison details are shown in **Figure 4**b and Table S1. Meanwhile, the electrochemical double-layer capacitances (C_{dl}) were measured to estimate the electrochemical surface areas (ECSA) of Ni-NM@G catalysts under non-Faradaic conditions. As shown in **Figure 4**c and Figure S10, the Ni-NM@G-10 catalyst exhibits considerably higher C_{dl} of 4.38 mF cm^{-2} than other catalysts, indicating more accessible active sites in Ni-NM@G-10. In contrast, An@G catalyst shows much lower C_{dl} (1.06 mF cm^{-2}) compared with Ni-NM@G catalysts. It further demonstrates that the introduction of Ni nanomeshes provides much more accessible active sites, which is beneficial for OER performance. Moreover, as shown in Figure

S11a, the OER activity of the sample prepared at 600 ^{o}C for 10 h (Ni-NM@G-600) is lower than Ni-NM@G-10 prepared at 550 ^{o}C, consistent with its significantly lower C_{dl} compared with Ni-NM@G-10 (Figure S11b). These can be attributed to the less amount of nickel nanomeshes in Ni-NM@G-600, which agrees well with the above discussion. Moreover, another control sample was prepared on Cu foam (denote as Cu-NM@G). As shown in Figure S12, the XPS spectrum of C 1s shows that the C-Br bond is also present in the catalyst. However, the OER performance of Cu-NM@G is close to An@G without the C-Br bond and much worse than Ni-NM@G. This result indicates that Br has no significant contribution in OER process and Ni embedded in the film should be responsible for the OER activity. High stability of an OER electrocatalyst is of great significance for the practical application. The chronopotentiometry was utilized to evaluate the electrocatalytic stability of Ni-NM@G catalysts for OER in 1.0 M KOH electrolyte. As shown in **Figure 4**d, the Ni-NM@G-10 shows negligible overpotential loss at 100 mA cm^{-2} for 50 h, indicating that it has an excellent stability for OER in alkaline media. After stability test, TEM images of the catalyst (Figure S13) evidence that interconnected nanoparticles (4~5 nm in diameter) are still uniformly embedded in graphene-like film. However, HRTEM image and XPS spectra suggest that the original metallic Ni nanoparticles should be oxidized into nickel (oxy)hydroxide or hydroxide during OER process (details see Supporting Information), which are commonly observed as the OER active sites in the literatures.[24]

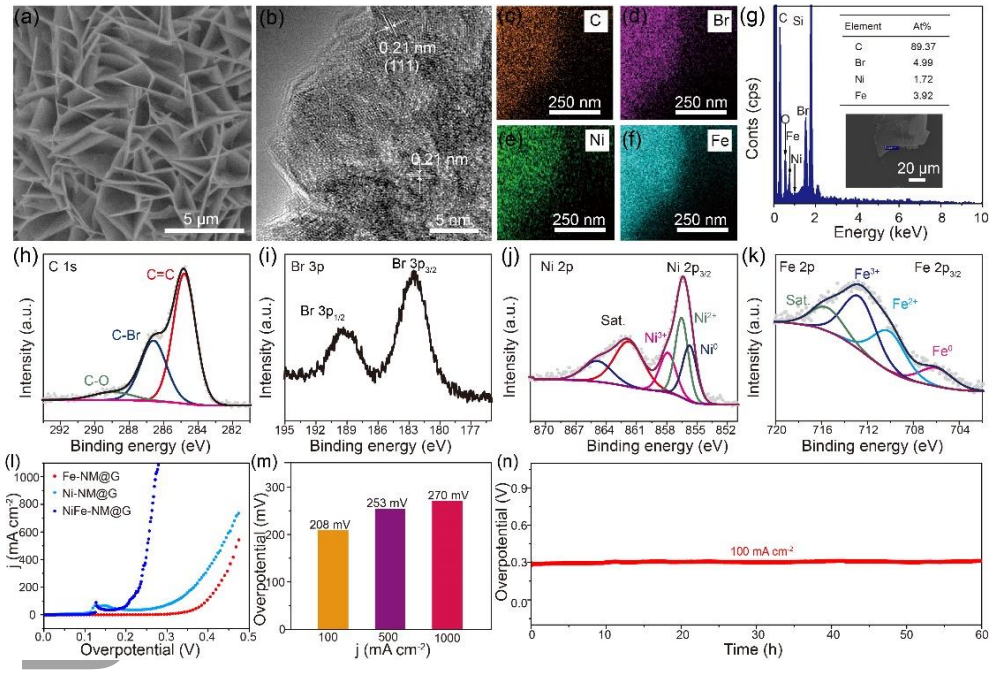

Figure 5. (a) SEM image, (b) HRTEM image, (c-f) TEM image and corresponding elemental mapping images, and (g) SEM image and EDS spectrum of NiFe-NM@G. (h-k) High-resolution XPS spectra of NiFe-NM@G: h) C 1s, i) Br 3p, j) Fe 2p and k) Ni 2p. (l) OER polarization curves in deaerated 1.0 M KOH solution at a scan rate of 2.0 mV s^{-1}. (m) Comparison of overpotentials at different current density. (n) Time-dependent current density curve for NiFe-NM@G in 1.0 M KOH.

Inspired by the solid migration mechanism, we extend this strategy to other bulk transition metal or alloy including Fe foam and NiFe foam for demonstrating its universality. The similar nanostructured functional electrocatalyst can be achieved on the Fe foam through the same procedures (noted as Fe-NM@G). The detailed information was described in Figure S14 and S15. Moreover, this strategy is also applicable for NiFe foam to give the product with similar morphology (noted as NiFe-NM@G). Accordingly, a series of catalysts on NiFe foam were prepared by controlling the growth time to monitor the solid migration of nickel and iron atoms under high temperature. It further confirms that the solid-phase migration of metal atom from transition metal foam substrate

is related to the active Br species. The detailed information was described in Figure S16-18. As shown in **Figure 5**a, the vertical nanosheet arrays is obtained on NiFe foam. The thickness of nanosheet is around 143.5 nm. The HRTEM image in **Figure 5**b shows lattice fringes with a spacing of 0.21 nm. Furthermore, the homogeneous distribution of C, Br, Ni, and Fe elements is detected in graphene-like carbon sheet by the elemental mapping experiments **(Figure 5**c-f). In addition, XPS spectra further confirmed the existence of C, Br, Ni and Fe elements (Figure S19). As shown in **Figure 5**h-k, it suggests the presence of metallic Ni and Fe as well as their oxidative states. Subsequently, the electrochemical experiments were carried out to evaluate the performance of these two catalysts for OER. As shown in **Figure 5**l, the Fe-NM@G exhibits the worst OER activity with an overpotential of 399 mV at 100 mA cm^{-2}, which is much higher than 318 mV for Ni-NM@G. However, this overpotential can be largely reduced to 208 mV on NiFe-NM@G. Notably, the industry-level current density of 500 and 1000 mA cm^{-2} can be achieved at ultrasmall overpotentials of 253 and 270 mV, respectively. Moreover, the NiFe-NM@G exhibits negligible overpotential loss for continuous operation at 100 mA cm^{-2} for 60 h (**Figure 5**n). Such extremely low overpotential and excellent stability make NiFe-NM@G ranking the top-tier OER catalysts. Meanwhile, as shown in Figure S20, the C_{dl} value of NiFe-NM@G is 3.38 mF cm^{-2}, close to those of Ni-NM@G (4.38 mF cm^{-2}) and Fe-NM@G (3.43 mF cm^{-2}). Accordingly, the OER current densities were normalized by ECSA as shown in Figure S21. It can be seen that NiFe-NM@G still greatly outperforms Ni-NM@G and Fe-NM@G. Furthermore, the electrochemical impedance spectroscopy (EIS) spectra of as-prepared catalysts and the equivalent circuit were shown in Figure S22. It can be seen that all the catalysts exhibit similar solution resistance (R_s) of 1.8 Ω, but a significantly distinct charge transfer resistances (R_{ct}). The NiFe-NM@G electrode shows the smallest R_{ct} value of about 6.6 Ω compared with Ni-

NM@G (12.2 Ω) and Fe-NM@G (16.6 Ω), indicating the fastest electron transfer kinetics of OER on NiFe-NM@G. This suggests that the high activity of NiFe-NM@G originates from the synergistic effect between Ni and Fe element, which is recognized in this field.[25] The above results conclude that our strategy of solid-phase migration for generating nanomeshes embedded in graphene-like films is versatile for activating various transition metal foam as highly efficient and durable OER electrocatalysts.

In summary, we demonstrate herein for the first time that organic small molecules such as hexabromobenzene can activate commercial bulk transition metals (such as Ni foam, Fe foam and NiFe foam) into highly-efficient OER electrocatalysts through Br-induced solid-phase migration to generate nanomeshes embedded in graphene-like films. The formation of conformal graphene-like network on transition metal foam from hexabromobenzene and the Br-induced extraction of transition metal atoms from substrate to generate transition metal nanomeshes integrated in the film have been systematically investigated. Thanks to the embedding of transition metal nanomeshes in graphene films, the abundant accessible active sites, and the on-substrate growth of graphene films for enhanced mechanical stability and protection of transition metal substrate from corrosion, the M-NM@G exhibits superior OER performance in terms of excellent long-term stability and low overpotentials to achieve industry-level current densities. For example, NiFe-NM@G can output 100 and 1000 mA cm^{-2} at the overpotentials of only 208 and 270 mV, respectively, ranking top in previous reports for water splitting. These results suggest that the present solid-phase migration activated by organic small molecules provides a general strategy to directly transform bulk transition metals into nanostructured functional materials, opening up a new avenue to produce high-performance electrocatalysts for diverse applications.

Experimental Section

Cleaning the substrate: Before loading the nickel foam into the quartz tube furnace, a thorough cleaning procedure was successively executed to remove any inorganic and/or organic impurities on the surface. It was cleaned with acetone, 10% HCl, and ethanol in turns and then dried under nitrogen flow.

Synthesis of M-NM@G catalysts: In the synthesis, all chemical reagents were analytical (AR) grade and were used as received without further purification. In order to control the sublimation rate of hexabromobenzene (HBB) and the growth rate of transition metal nanomeshes embedded in graphene-like films (M-NM@G), the HBB powders were pressed into a flake at room temperature with 15 Mpa pressure. Based on above steps, a piece of 300 mg HBB flake was placed in the center of heating zone and transition metal foam was put in the growth zone. The HBB vapor was introduced by the 500 sccm Ar. As for Ni foam, the typical growth time was 1, 5 and 10 hours. The typical growth temperature was 550 ^{o}C and 600 ^{o}C. The catalysts were defined by different growth time and temperature, which were named Ni-NM@G-1, Ni-NM@G-5, Ni-NM@G-10, and Ni-NM@G-600, respectively. As for Fe foam, Cu foam and NiFe foam, the growth condition was same as Ni foam, which were noted Fe-NM@G, Cu-NM@G and NiFe-NM@G, respectively.

Synthesis of An@G catalyst: Anthracene (An) is another organic small molecules with similar structure to HBB but without C-Br bonds. A piece of 300 mg An flake was placed in the center of heating zone and nickel foam was put in the growth zone. The HBB vapor was introduced by the 500 sccm Ar. The typical growth condition was same as Ni foam. The catalyst was defined as An@G.

Characterizations

The as-prepared M-NM@G catalysts were characterized by a Hitachi S-4800 field emission scanning electron microscope (SEM) operating at 10 kV combined with energy-dispersive X-ray spectroscopy (EDS). Transmission electron microscopy (TEM), high-resolution (HRTEM) and cross-section transmission electron microscopy were recorded on a JEOL JEM-2100F microscope operating at 200 kV. Elemental mapping was performed with an EDS detector equipped on the JEOL-2100F TEM. X-ray photoelectron spectroscopy (XPS) was recorded on a Thermo Scientific ESCA Lab250xi using an Mg Kα X-ray as the excitation source. The binding energies were referenced to C 1s line at 284.8 eV from adventitious carbon. The Raman spectroscopy was recorded on a Thermo Scientific DXR with a 532 nm laser wavelength. The EDS results in this work were conducted on nickel nanomeshes exfoliated from M-NM@G catalysts. Powder XRD patterns were recorded on a Regaku D/Max-2500 diffractometer equipped with a Cu Kα1 radiation (λ=1.54056 Å) at a scan rate of 4° min^{-1}. FTIR spectroscopy was carried out on an iN10-iZ10 FTIR spectrometer.

Oxygen Evolution Reaction (OER) measurements

All electrochemical tests were conducted on an electrochemical workstation CHI 660E. Using a conventional three-electrode cell in 1.0 M KOH electrolyte. The as-prepared electrodes, Hg/HgO electrode (1.0 M KOH), and carbon rod were used as working electrode, reference electrode, and counter electrode, respectively. All measured potentials were converted to the reversible hydrogen electrode (RHE), according to the equation:

$$E_{\mathrm{RHE}} = E_{Hg/HgO} + 0.098 + 0.059 * \mathrm{pH}$$

The linear sweep voltammetry (LSV) curves were recorded at a scan rate of 2 mV s^{-1}. All curves were recorded with 85% iR-compensation unless specified. The long-term stability test was performed using chronopotentiometry method at a constant current density. The C_{dl} values for as-prepared working electrodes were determined from the cyclic voltammogram (CV) in the double layer region (without faradaic processes) at different scan rates. Electrochemical impedance spectroscopy was carried out in a frequency range from 100 KHZ to 0.01 HZ and amplitude of 5 mV. For excluding the influence of ECSA on the performance, the OER performance was normalized by ECSA. The ECSA-normalized current density for as-prepared catalysts was calculated according to :

ECSA-normalized current density = current density × C_S/C_{dl}

C_S is the specific capacitance. In this work, 0.040 mF cm^{-2} was adopted as the value of Cs on a basis of previously reported OER catalysts in alkaline.

Supporting Information

Supporting Information is available from the Wiley Online Library or from the author.

Acknowledgements

J. Zhang and W.-J. Jiang contributed equally to this work. This work was supported by the Ministry of Science and Technology of China (2017YFA0204704, 2016YFB0401100, and 2016YFB0101202), National Natural Science Foundation of China (21805284, 21873108, and 21773263), and Chinese Academy of Sciences (Hundred Talents Plan and Youth Innovation Promotion Association) (Grant No. XDPB0602).

Received: ((will be filled in by the editorial staff))
Revised: ((will be filled in by the editorial staff))
Published online: ((will be filled in by the editorial staff))

References

[1] a) M. Lefèvre, E. Proietti, F. Jaouen, J.-P. Dodelet, *Science* **2009**, 324, 71; b) J. R. McKone, E. L. Warren, M. J. Bierman, S. W. Boettcher, B. S. Brunschwig, N. S. Lewis, H. B. Gray, *Energy Environ. Sci.* **2011**, 4, 3573; c) X. Huang, Z. Zeng, H. Zhang, *Chem. Soc. Rev.* **2013**, 42, 1934; d) S. Zhao, Y. Wang, J. Dong, C.-T. He, H. Yin, P. An, K. Zhao, X. Zhang, C. Gao, L. Zhang, J. Lv, J. Wang, J. Zhang, A. M. Khattak, N. A. Khan, Z. Wei, J. Zhang, S. Liu, H. Zhao, Z. Tang, *Nat. Energy* **2016**, 1, 16184; e) G. Fu, Z. Cui, Y. Chen, Y. Li, Y. Tang, J. B. Goodenough, *Adv. Energy Mater.* **2017**, 7, 1601172.

[2] a) L. Zhang, J. Fischer, Y. Jia, X. Yan, W. Xu, X. Wang, J. Chen, D. Yang, H. Liu, L. Zhuang, M. Hankel, D. J. Searles, K. Huang, S. Feng, C. L. Brown, X. Yao, *J. Am. Chem. Soc.* **2018**, 140, 10757; b) X.-L. Wang, L.-Z. Dong, M. Qiao, Y.-J. Tang, J. Liu, Y. Li, S.-L. Li, J.-X. Su, Y.-Q. Lan, *Angew. Chem. Int. Ed.* **2018**, 57, 9660; c) Z. Zhao, H. Liu, W. Gao, W. Xue, Z. Liu, J. Huang, X. Pan, Y. Huang, *J. Am. Chem. Soc.* **2018**, 140, 9046; d) E. M. Wiensch, J. Montgomery, *Angew. Chem. Int. Ed.* **2018**, 57, 11045; e) Y. Li, W. Zhou, H. Wang, L. Xie, Y. Liang, F. Wei, J.-C. Idrobo, S. J. Pennycook, H. Dai, *Nat. Nanotechnol.* **2012**, 7, 394.

[3] a) W. Zhou, X.-J. Wu, X. Cao, X. Huang, C. Tan, J. Tian, H. Liu, J. Wang, H. Zhang, *Energy Environ. Sci.* **2013**, 6, 2921; b) L. Xie, R. Zhang, L. Cui, D. Liu, S. Hao, Y. Ma, G. Du, A. M. Asiri, X. Sun, *Angew. Chem. Int. Ed.* **2017**, 56, 1064; c) T. Tang, W.-J. Jiang, S. Niu, N. Liu, H. Luo, Q. Zhang, W. Wen, Y.-Y. Chen, L.-B. Huang, F. Gao, J.-S. Hu, *Adv. Funct. Mater.* **2018**, 28, 1704594.

[4] F. Yu, H. Zhou, Z. Zhu, J. Sun, R. He, J. Bao, S. Chen, Z. Ren, *ACS Catal.* **2017**, 7, 2052.

[5] X. Liu, W. Liu, M. Ko, M. Park, M. G. Kim, P. Oh, S. Chae, S. Park, A. Casimir, G. Wu, J. Cho, *Adv. Funct. Mater.* **2015**, 25, 5799.

[6] a) X. Zhou, Z. Xia, Z. Zhang, Y. Ma, Y. Qu, *J. Mater. Chem. A* **2014**, 2, 11799; b) M. Gao, W. Sheng, Z. Zhuang, Q. Fang, S. Gu, J. Jiang, Y. Yan, *J. Am. Chem. Soc.* **2014**, 136, 7077; c) J. Xie, X. Zhang, H. Zhang, J. Zhang, S. Li, R. Wang, B. Pan, Y. Xie, *Adv. Mater.* **2017**, 29, 1604765.

[7] a) S. Niu, W.-J. Jiang, T. Tang, Y. Zhang, J.-H. Li, J.-S. Hu, *Adv. Sci.* **2017**, 4, 1700084; b) D. Friebel, M. W. Louie, M. Bajdich, K. E. Sanwald, Y. Cai, A. M. Wise, M.-J. Cheng, D. Sokaras, T.-C. Weng, R. Alonso-Mori, R. C. Davis, J. R. Bargar, J. K. Norskov, A. Nilsson, A. T. Bell, *J. Am. Chem. Soc.* **2015**, 137, 1305.

[8] W.-J. Jiang, S. Niu, T. Tang, Q.-H. Zhang, X.-Z. Liu, Y. Zhang, Y.-Y. Chen, J.-H. Li, L. Gu, L.-J. Wan, J.-S. Hu, *Angew. Chem. Int. Ed.* **2017**, 56, 6572.

[9] a) X. Jia, Y. Zhao, G. Chen, L. Shang, R. Shi, X. Kang, G. I. N. Waterhouse, L.-Z. Wu, C.-H. Tung, T. Zhang, *Adv. Energy Mater.* **2016**, 6, 1502585; b) Y. Wang, Y. Zhang, Z. Liu, C. Xie, S. Feng, D. Liu, M. Shao, S. Wang, *Angew. Chem. Int. Ed.* **2017**, 56, 5867.

[10] K. Xu, P. Chen, X. Li, Y. Tong, H. Ding, X. Wu, W. Chu, Z. Peng, C. Wu, Y. Xie, *J. Am. Chem. Soc.* **2015**, 137, 4119.

[11] T. Tang, W.-J. Jiang, S. Niu, N. Liu, H. Luo, Y.-Y. Chen, S.-F. Jin, F. Gao, L.-J. Wan, J.-S. Hu, *J. Am. Chem. Soc.* **2017**, 139, 8320.

[12] Y. Qu, Z. Li, W. Chen, Y. Lin, T. Yuan, Z. Yang, C. Zhao, J. Wang, C. Zhao, X. Wang, F. Zhou, Z. Zhuang, Y. Wu, Y. Li, *Nat. Catal.* **2018**, 1, 781.

[13] L. Jiang, T. Niu, X. Lu, H. Dong, W. Chen, Y. Liu, W. Hu, D. Zhu, *J. Am. Chem. Soc.* **2013**, 135, 9050.

[14] X. Liu, I. S. Amiinu, S. Liu, K. Cheng, S. Mu, *Nanoscale* **2016**, 8, 13311.

[15] a) K. Zhang, J. Huang, W. Zhang, Y. Yu, S. Deng, G. Yu, *J. Hazard. Mater.* **2012**, 243, 278; b) B. J. Rani, K. Nivedha, G. Ravi, R. Yuvakkumar, *ChemistrySelect* **2019**, 4, 10122.

[16] J. Zhong, L. Song, Z.-Y. Wu, S.-S. Xie, M. Abbas, K. Ibrahim, H. Qian, *Carbon* **2006**, 44, 866.

[17] F. Sun, G. Wang, Y. Ding, C. Wang, B. Yuan, Y. Lin, *Adv. Energy Mater.* **2018**, 8, 1800584.

[18] H. Xu, Z.-X. Shi, Y.-X. Tong, G.-R. Li, *Adv. Mater.* **2018**, 30, 1705442.

[19] H. Liang, F. Meng, M. Caban-Acevedo, L. Li, A. Forticaux, L. Xiu, Z. Wang, S. Jin, *Nano Lett.* **2015**, 15, 1421.

[20] Z. Peng, D. Jia, A. M. Al-Enizi, A. A. Elzatahry, G. Zheng, *Adv. Energy Mater.* **2015**, 5, 1402031.

[21] Y. Han, Y. Yu, L. Zhang, L. Huang, J. Zhai, S. Dong, *Talanta* **2018**, 186, 154.

[22] J. S. Chen, J. Ren, M. Shalom, T. Fellinger, M. Antonietti, *ACS Appl. Mater. Interfaces* **2016**, 8, 5509.

[23] M. Ledendecker, G. Clavel, M. Antonietti, M. Shalom, *Adv. Funct. Mater.* **2015**, 25, 393.

[24] a) C. Tang, N. Cheng, Z. Pu, W. Xing, X. Sun, *Angew. Chem. Int. Ed.* **2015**, 54, 9351; b) M. W. Louie, A. T. Bell, *J. Am. Chem. Soc.* **2013**, 135, 12329; c) X. Xu, F. Song, X. Hu, *Nat. Commun.* **2016**, 7, 12324.

[25] S. Niu, W.-J. Jiang, Z. Wei, T. Tang, J. Ma, J.-S. Hu, L.-J. Wan, *J. Am. Chem. Soc.* **2019**, 141, 7005.

Transition Metal nanomeshes embedded in graphene-like film are achieved via a newly-developed Br-induced solid-phase migration method enabled by directly treating commercial transition metal foam with organic small molecule. NiFe-NM@G exhibits excellent OER performance with a low overpotential of 208 mV at a current density of 100 mA cm^{-2} as well as excellent long-term stability.

Keywords: transition metal nanomesh, graphene-like film, solid-phase migration, hexabromobenzene, oxygen evolution reaction

Jing Zhang, Wen-Jie Jiang, Shuai Niu, Hantang Zhang, Jie Liu, Haiyang Li, Gui-Fang Huang, Lang Jiang, Wei-Qing Huang*, Jin-Song Hu*, and Wenping Hu*

Organic Small Molecule Activates Transition Metal Foam for Efficient Oxygen Evolution Reaction